ARTICLE IN PRESS

Ceramics International xxx (xxxx) xxx

Contents lists available at ScienceDirect

Ceramics International

journal homepage: www.elsevier.com/locate/ceramint

# Correlations of structural, thermal and electrical properties of sodium doped complex borophosphosilicate glass

Zuzanna Milewczyk [a], Sharafat Ali [b], Piotr Okoczuk [a], Jacek Ryl [a], Ryszard J. Barczyński [a], Natalia A. Wójcik [a,b,*]

[a] Institute of Nanotechnology and Materials Engineering, Faculty of Applied Physics and Mathematics, Gdańsk University of Technology, Narutowicza Street 11/12, 80–233, Gdańsk, Poland

[b] Department of Built Environment and Energy Technology, Linnaeus University, 35195 Växjö, Sweden

ARTICLE INFO

Handling Editor: Dr P. Vincenzini

*Keywords:*
Borophosphosilicate
High sodium content
Thermal properties
IR spectroscopy
Impedance spectroscopy

ABSTRACT

Borophosphosilicate glasses with varying sodium ion concentrations were investigated for their, structural, thermal, and electrical properties. All the obtained glasses were transparent except the glass with the highest sodium content, which exhibited translucency due to inhomogeneities. Increasing sodium content led to reduced boron and silicon content while maintaining a constant B/Si ratio, indicating progressive depolymerization of the glass network. Confocal microscopy, scanning electron microscopy, and atomic force microscopy showed homogeneous and granular structure for samples with lower sodium content, but higher sodium content resulted in visible agglomeration/nanocrystallization. X-ray diffractograms showed amorphous nature for most samples, with samples doped with the highest concentrations of $Na_2O$ showing several broad reflections suggesting nanoscale crystallinity. Fourier-transform infrared spectroscopy revealed shifts in dominant bands with increasing sodium content, indicating depolymerization of the borate network. An observed decrease in glass transition temperature and thermal stability with increasing sodium content was attributed to depolymerization and formation of non-bridging oxygens. Impedance spectroscopy revealed two relaxation processes associated with the transport of $Na^+$ ions through two different regions. DC conductivity and activation energy predominantly increased with the sodium ion content at high temperatures.

## 1. Introduction

Borate glasses are characterized by low melting temperature and exhibit interesting properties such as chemical resistance, optical transparency, and electrical insulation in their pure form, making them highly desirable materials for a variety of applications including solar energy converters, optical fibers, electronics, and radiation shielding [1-4]. The glass network of borate glasses is composed of two types of coordination with oxygen atoms, resulting in trigonal and tetragonal units. The small $B^{3+}$ ion allows to fit precisely into the triangular void created by the contact of three oxide ions, leading to the formation of $BO_3$ units. These units, arranged in triangular configurations, offer various glass structure combinations such as di-, tri-, tetra- and penta-, facilitated by the introduction of appropriate modifiers and linked by B–O–B bonds. $BO_3$ units serve as the basic building blocks of all borate-based glasses, and the addition of a network modifier can additionally improve the physical and structural properties of these glasses [4-6]. Alkali ions, including: $Na^+$, $Li^+$, $K^+$, $Rb^+$, and $Cs^+$, act as a modifier in the borate network. However, their adequate concentration can change the dielectric material into ionic semiconductor [7-10]. The ionic conductivity of glasses results from the hopping of monovalent cations under the influence of an applied electric field [11,12]. Na–B–O glass systems may exhibit high ionic conductivity therefore they can be a good candidate for solid electrolytes for new generation sodium-batteries [13-15]. It is worth mentioning that soda-borate glasses are highly hygroscopic, therefore doping with other network-building oxides like $SiO_2$ will be beneficial to improve chemical resistance and mechanical stability [16,17].

One of the well-studied glasses are soda-lime-silicate glasses [18-21]. Their electrical properties depends on the $Na_2O$ content, reaching approximately $3 \times 10^{-3}$ Scm$^{-1}$ at 300 °C for a 50 mol% content. This increase could be attributed to the structure changes caused by higher

* Corresponding author. Institute of Nanotechnology and Materials Engineering, Faculty of Applied Physics and Mathematics, Gdańsk University of Technology, Narutowicza Street 11/12, 80–233 Gdańsk, Poland.

*E-mail address:* natalia.wojcik@pg.edu.pl (N.A. Wójcik).

https://doi.org/10.1016/j.ceramint.2024.05.289
Received 28 February 2024; Received in revised form 28 April 2024; Accepted 18 May 2024
Available online 19 May 2024


Please cite this article as: Zuzanna Milewczyk et al., *Ceramics International*, https://doi.org/10.1016/j.ceramint.2024.05.289

concentration of modifier oxide, which enhance the mobility of the monovalent cations [22]. The impact of the modifications of glass structure and composition on conductivity behavior in silicate glass system remain of great interest. The studies of the effect of substituting CaO for $Na_2O$ in silicate glasses, demonstrating that it modifies the glass network and increases conductivity values not only by the higher mobile ion content but also because of an improvement of its mobility [23]. Research on the influence of changes in the silicate glass matrix while maintaining a constant content of alkali ions showed that the conductivity of glasses doped with, among others, Ca, Mg, Ge are reduced [24,25]. A similar effect was observed in the case of substitution with Ti, Ge, Zr, Sn and Ce cations. The decrease in conductivity was related to the impact of the added cations on the mobility of moving $Na^+$ ions [26]. Depending on the dopants, silicate glasses are characterized by high melting point, glass transition, chemical resistance and good mechanical parameters. They are often the basic element of glasses used in everyday life [18,22,24,27,28]. For this reason, it is worth considering their addition to borate glasses to improve their target properties. In a review summarizing the progress made thus far in the quest for sodium glasses with high ionic conductivity for emerging battery technologies, it becomes apparent that many glasses and glass-ceramics exhibiting such conductivity, apart from $SiO_2$, also incorporate glass-forming oxides like $P_2O_5$ [14,17,29-32]. There are suggestions that the presence of the amorphous or crystalline phosphate phase could significant enhance the ionic conductivity of the glasses therefore it was also included it in the structure of the studied materials [14,17,29-33].

Presented findings highlight the significant influence of sodium doping on the structural, thermal, and electrical properties of borophosphosilicate glasses, emphasizing the importance of understanding composition-property relationships in this glass system. Therefore, the aim of this study is to determine the ionic conductivity of mentioned glass system doped with high sodium ion content. Furthermore, a thorough structure analysis, correlated with thermal behavior, is provided to enhance understanding of the ion transport mechanism.

## 2. Experimental

Five glass samples were prepared by melt-quenching technique with different chemical composition $xNa_2O–2P_2O_5$-(98-x)[$2B_2O_3–SiO_2$], with x = 49, 43, 40, 37 and 31 in mol%. The batch materials used in glass melting were $Na_2HPO_4$ (≥99.5 % Sigma Aldrich), $Na_2CO_3$ (99.9+ % ChemPur GmbH), $H_3BO_3$ (Alfa Aesar 99.5 %) and $SiO_2$ (99.9 %, ABCR GmbH & Co.). The mixed batch materials were ground in an agate mortar, then melted in alumina crucible in air at a temperature of 950 °C for approximately 30 min. The glasses were poured onto a brass plate preheated to 250 °C and stamped to obtain flat samples. To remove internal stresses, the glasses were annealed at a temperature of 330°C for 10h with a heating and cooling rate of 3°Cmin$^{-1}$.

The compositions of the obtained samples were determined using a Scanning Electron Microscope (SEM), FEI Company Quanta FEG250 with an Energy Dispersive X-ray Spectrometer (EDX GENESIS Apex Apollo X60 Spectrometer). EDX measurements were performed in three different areas of fresh cross-sections for each sample. The obtained results were similar, and average values were used to estimate the metal contents. The boron content was estimated by keeping the Na/Si and Na/P ratios constant. The content of all metals is shown with an accuracy of ±3 %. All figures and calculations in this paper are made using the analyzed compositions. The morphology of glass surfaces was examined using an Olympus LEXT OLS4000 Confocal Scanning Laser Microscope (CSLM). Color imaging was executed under white LED light, while 3D images were acquired utilizing a 405 nm laser and a Photomultiplier Detector. The highest optical magnification employed was 2160x.

All the samples were investigated using the X-ray powder diffraction (XRPD) method. Spectra were obtained at room temperature, employing a Bruker D2 PHASER diffractometer equipped with CuKα radiation (wavelength, λ = 1.5406 Å) and a LynxEye-XE detector, covering a 2θ range of 5° to 70°. Additionally, the samples structure were assessed using infrared (IR) spectroscopy. Powdered samples, blended with KBr powder, were pressed using a hydraulic press to form plane-parallel plates. Fourier-transform infrared (FTIR) spectrum were recorded using a PerkinElmer FTIR spectrometer with scanning range of 400–4000 cm$^{-1}$, averaging 64 scans, and a resolution of 4 cm$^{-1}$. The acquired IR spectra underwent background correction and normalization to the dominant band. The band positions were determined using Origin software with a precision of ±2 cm$^{-1}$.

The thermal properties were examined by differential scanning calorimetry (DSC) using a Phoenix DSC 204 F1 Netzsch instrument for a sample mass of approximately 5 mg. Measurements were performed in alumina crucibles with a lid, under the air flowing, at a heating rate of 10°Cmin$^{-1}$ from a temperature of 30–600°C. Proteus software from NETZSCH was used to estimate the glass transition temperature ($T_g$) and crystallization process temperatures ($T_c$), with an accuracy of ±2 %.

The electrical properties of the samples were studied using the impedance spectroscopy technique. Gold electrodes were deposited onto the finely polished, plane-parallel surfaces of circular samples under vacuum. Impedance assessments were conducted over a frequency range spanning from 10 mHz to 1 MHz and a temperature range of 473 K–153 K, with a step of 10K (during cooling). An AC voltage of 1 $V_{rms}$ was applied during the measurements utilizing the Novocontrol Concept 40 broadband dielectric spectrometer Alpha-A, equipped with the ZG4 dielectric interface. The measurements were carried out in a nitrogen atmosphere, employing the temperature control system Quatro Cryosystem.

## 3. Results and discussion

### 3.1. Glass composition, topography and structure

Glasses obtained in the borophosphosilicate system with varying concentrations of sodium ions are colorless and transparent, as shown in Fig. 1. Among all these glasses, only the one with the highest sodium content is translucent, indicating the presence of inhomogeneities within it. Despite being exposed to atmospheric factors for a long period (a year), the samples did not show clear hygroscopic properties, suggesting an improvement in chemical resistance due to the addition of $SiO_2$. Table 1 shows the ID's of the samples associated with the $Na_2O$ content in mol% (31, 37, 40, 43, or 49) and their compositions before and after melting. However, attempts to melting sample 49Na into a stable format were unsuccessful due to high internal stresses, resulting the immediate cracking of the sample. The increasing content of sodium oxide in the samples replaced both boron and silicon oxides, the ratio of which remained constant at 3.8. Therefore, as a result, with the increase in the Na content (from 17.3 at% to 26.9 at%) a decrease in the B content (from 21.2 %at to 16.4 %at) and a slight decrease in the Si content (from 5.5 at% to 4.4 %at) were mostly observed. Additionally, during the melting process, all glasses dissolved alumina from the crucible material, which was taken into account in the analyzed compositions (Table 1). Notably, the maximum alumina content did not exceed approximately 1 at%. Comparing the theoretical batch compositions with the obtained glass ones, a gradual increase in the sodium content was observed along with a simultaneous decrease in the content of B and Si, i.e. the main units building the glass structure. However, the EDX


**Fig. 1.** The photograph showing as-quenched samples.

**Table 1**
Glasses IDs, target and evaluated compositions.

| Sample ID | Target glass composition (in at %) | Evaluated glass composition (in at %) |
|---|---|---|
| **$xNa_2O–2P_2O_5$-(98-x) [$2B_2O_3–SiO_2$] in mol%** | | |
| 31Na | $Na_{15.7}B_{22.2}Si_{5.8}P_1O_{55.3}$ | $Na_{17.3}B_{21.2}Si_{5.5}P_1Al_{0.4}O_{54.6}$ |
| 37Na | $Na_{19.1}B_{20.6}Si_{5.4}P_1O_{53.9}$ | $Na_{20.9}B_{19.1}Si_5P_1Al_1O_{53}$ |
| 40Na | $Na_{20.8}B_{19.8}Si_{5.2}P_1O_{53.1}$ | $Na_{21.7}B_{19.1}Si_5P_1Al_{0.4}O_{52.7}$ |
| 43Na | $Na_{22.6}B_{18.9}Si_5P_{1.1}O_{52.4}$ | $Na_{24.3}B_{17.6}Si_{4.6}P_1Al_{0.9}O_{51.6}$ |
| 49Na | $Na_{26.3}B_{17.2}Si_{4.6}P_{1.1}O_{50.8}$ | $Na_{26.9}B_{16.4}Si_{4.4}P_{0.9}Al_1O_{50.5}$ |

results are very close to the nominal glasses compositions, with differences of only 1–2 at%. Therefore, the higher sodium content in the obtained composition may be due to normalizing the EDX results to 100 %, while also accounting for the additional aluminum presence.

Fig. 2 illustrates micrographs obtained by confocal microscopic technique for all samples: (A) 31Na, (B) 37Na, (C) 40Na, (D) 43Na, and (E) 49Na, at lower (left) and higher (right) magnifications. Upon analyzing the surface topography, it becomes apparent that the 31Na, 37Na, and 40Na samples are homogeneous, with no visible areas of phase separation or agglomeration [34-36]. Such morphologies are typical for glasses. The topography of sample 43Na differs from the previous ones by the presence of visible dark point structures distributed over the entire tested surface. These observations may indicate a possible phase separation phenomenon, which is sometimes observed in glasses composed of multiple oxides forming a glass network [37,38], and/or agglomeration of a specific phase, not necessarily glass-forming. This phenomenon of phase separation/agglomeration was not observed in samples with a lower sodium oxide content, suggesting that the amount of sodium ions may significant impact the topography and behavior of the glass network. There is no dominant homogeneous structure in 49Na sample, which emphasizes the heterogeneity of the surface. Numerous precipitations are evident on the sample surface, and the formation of regular crystal structures indicates an ongoing crystallization process during the cooling of the melt.

To verify whether the visible inhomogeneities are only a surface effect and whether the structure of the glasses is homogeneous inside the material, further microstructure analysis was performed using the SEM technique. Fig. 3 shows micrographs captured on fresh fractures at various sample locations: 31Na (A), 37Na (B), 40Na (C), and D)), 43Na (E), and F)), and 49Na (G), and H)). Tests performed at lower magnifications showed that samples 31Na, 37Na, 40Na and 43Na are homogeneous at the fractures. However, at higher magnifications, samples 31Na (Fig. 3A) and samples 37Na (Fig. 3B) exhibit a granular structure. For comparison, fragments of fractures for samples 40Na (Fig. 3C) and 43Na (Fig. 3F) are presented at similar magnifications, where such granularity was not observed. However, in these samples, depending on the measurement location, some larger spherical inhomogeneities are observed. In the 43Na sample (Fig. 3E), circular-shaped inhomogeneities can be seen, with diameter reaching up to 100 nm. The inhomogeneities are distributed unevenly within the homogeneous matrix. Measurement of the 40Na sample on the oblique part of the fracture showed the presence of size inhomogeneities reaching even μm (Fig. 3D, marked with red frame 1). However, they were not visible on the flat part of the sample. EDX analysis showed that these inhomogeneities were richer in sodium than the surrounding matrix. The Na/Si ratio in red area 1 was 5.4, and in red area 2 was 4.5 (for comparison, in the 40Na composition Na/Si is 4.34). The 49Na sample was heterogeneous throughout, with smaller and bigger inhomogeneities ranging in size from nano to microscale (Fig. 3G and H).

Additionally, observations were conducting using AFM, and the results are summarized in Fig. 4 for fresh fractured samples: 31Na (A), 37Na (B), 40Na (C), 43Na (D), and 49Na (E) and (F)). Samples 31Na and 37Na are characterized by a flat surface, with changes in height reach 9–11 nm. Some granularity of the structure is visible, similarly to the SEM results. The results were consistent across different measurement locations. For the 40Na sample, some difference in topography begins to become visible. Depending on the location of measurement, the presence of larger or smaller inhomogeneities was observed. However, samples 43Na and 49Na show significantly different topography. Some inhomogeneities are visible, with their content increases significantly in the case of the 49Na sample. Based on the described topography studies on the surface and fractures, it can be concluded that the 31Na and 37Na samples tend to agglomerate, most likely of the sodium-rich phase. When sodium levels exceed a certain threshold (21 at%), agglomeration begins, possibly leading to nano/micro-crystallization.

XRD studies were performed to determine the presence of a crystalline phase in the samples. X-ray diffractograms for all samples are presented in Fig. 5. The results for samples 31Na, 37Na, 40Na, 43Na showed halo typical of amorphous materials, with no intense reflections related to the crystalline phase. However, the diffractogram of sample 49Na shows broad and relatively low-intensity single reflections, suggesting the possible presence of a crystalline phase on the nanometer scale. The width and the surrounding amorphous halo make it challanging to assign them to a specific crystalline phases. Nevertheless, they are most likely assosiated with $SiO_2$ (code: 01-083-1831, ICSD:100753

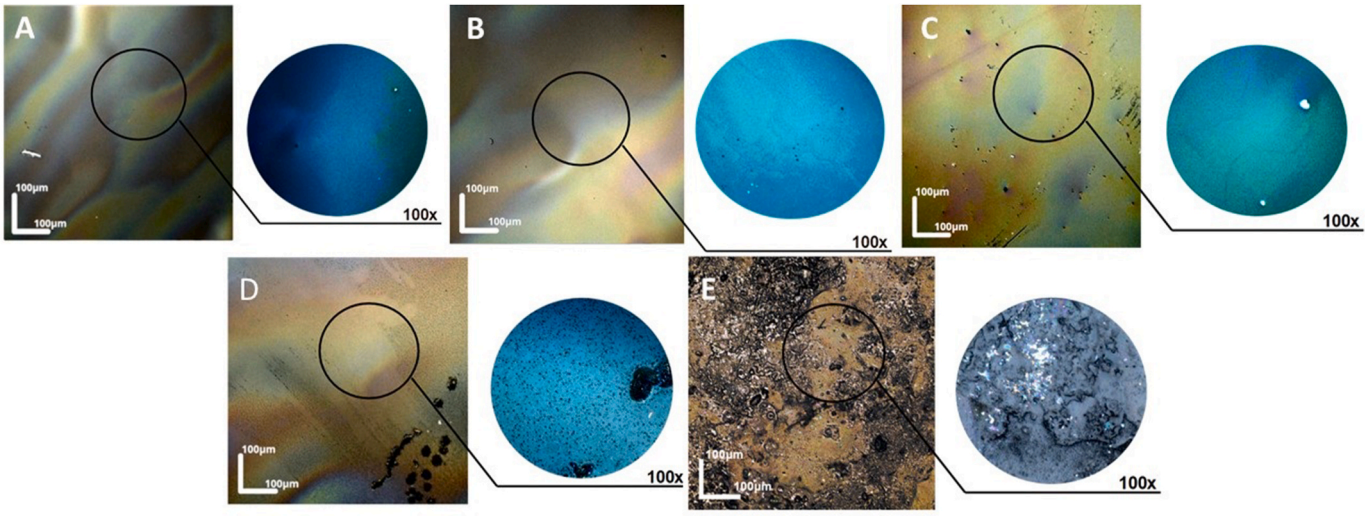


**Fig. 2.** Topography of glasses: (A) 31Na, (B) 37Na, (C) 40Na, (D) 43Na, and (C) 49Na observed using a confocal microscope, at lower (left) and higher (right) magnifications.

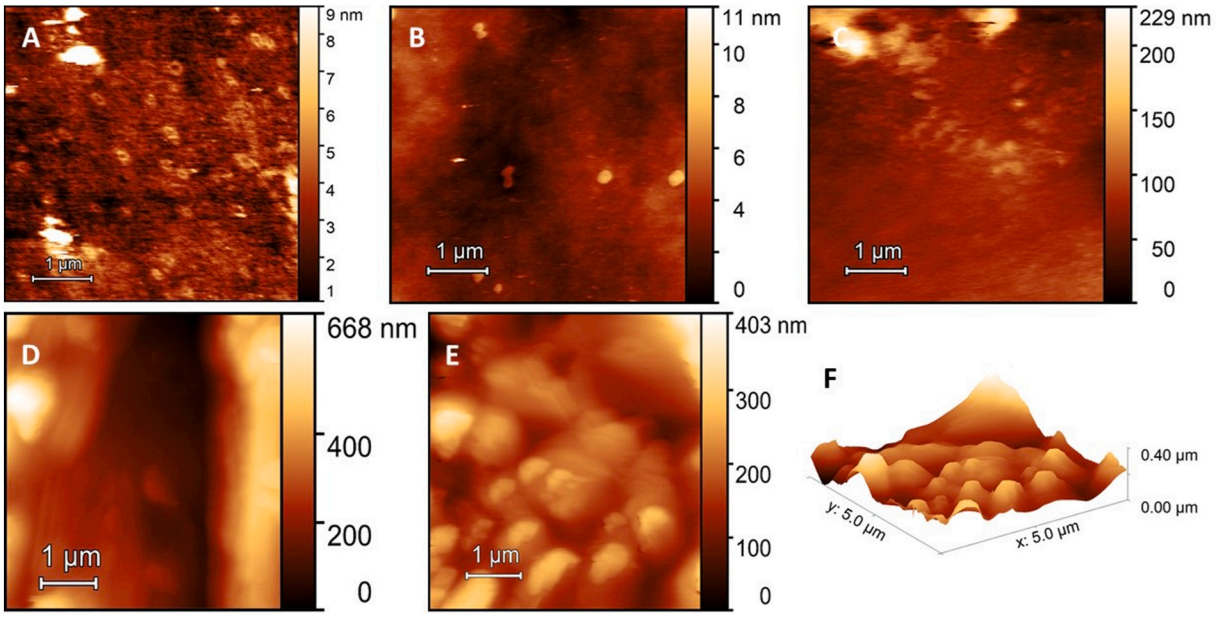


**Fig. 3.** SEM micropgraphs of fresh cross-sections of samples: A) 31Na, B) 37Na, C), and D) 40Na, E), and F) 43Na, and G), and H) 49Na.

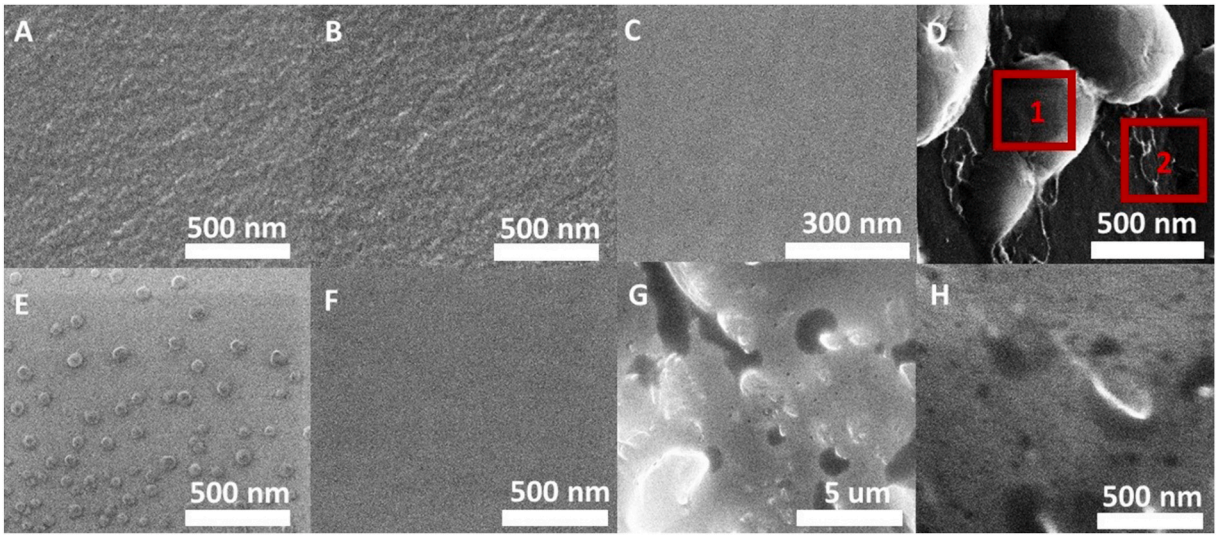


**Fig. 4.** AFM micrographs of fresh cross-sections for the samples: A) 31Na, B) 37Na, C) 40Na, D) 43Na, and E) 49Na. F) shows morphology of sample 49Na in 3D.

[39]) and $Na_4P_2O_7$ (code: 00-010-0187, ICSD 10370 [40]). Based on the reflections' width, it can be estimated that the size of the observed crystallites is lower than 20 nm [41]. The diffractograms of the remaining samples show some changes in appearance, which may also suggest the presence of a nanocrystalline phase, especially in the 43Na and possibly 40Na samples. However, these effects are barely visible and the position of these possible reflections is impossible to identify using our software. On this basis, we are unable to clearly deny or confirm possible nanocrystallinity in the mentioned materials.

The IR spectra for all specimen are plotted in Fig. 6A. It can be seen that the visible bands are mostly rounded, characteristic of the amorphous phase. The main bands correlated with the glass network are found in the range of 400–1600 $cm^{-1}$. Analysis of the IR spectra of all glass samples reveals a significant shift of the dominant bands with increasing sodium content. Therefore, we will first describe the spectrum for the sample with the lowest sodium content (31Na) to attribute the observed changes to the increasing modifier content. The dominant visible band is wide, and extends from ~750 $cm^{-1}$ to above 1200 $cm^{-1}$, and is associated with the main units forming the glass network. Its asymmetry indicates that it consists of several smaller bands. Taking this into account, the most intense band can be distinguished at 982 $cm^{-1}$, with a visible shoulder at 846 $cm^{-1}$ and symmetrically at 1094 $cm^{-1}$. Additionally, a slightly visible bulge around 1190 $cm^{-1}$ can be observed. Considering that the main units building the glass network are borate units, and the asymmetric stretching vibrations of $BO_4$ units are centered in the range of 800–1200 $cm^{-1}$, it can be assumed that the dominant bands are related to the B–O vibrations of $BO_4$ units [42,43]. The band observed at 1094 $cm^{-1}$ can be correlated with di-, tri-,tetra-, and pentaborate groups belonging to $BO_3$ and $BO_4$ units [42,43]. Also visible shoulders close to 1190 $cm^{-1}$ and 846 $cm^{-1}$ are typical for to B–O stretching vibrations of trigonal ($BO_3$, $BO_2O^-$) units [44,45]. It is worth noting that the second phase that builds the glass network to a relatively lesser extent is silicate units, which exhibits activity in a similar range of wavenumber. Therefore, the possibility of attributing few bands due to the presence of Si–O bonds should be considered. The main band may result from the overlapping activity of borate units and the stretching of

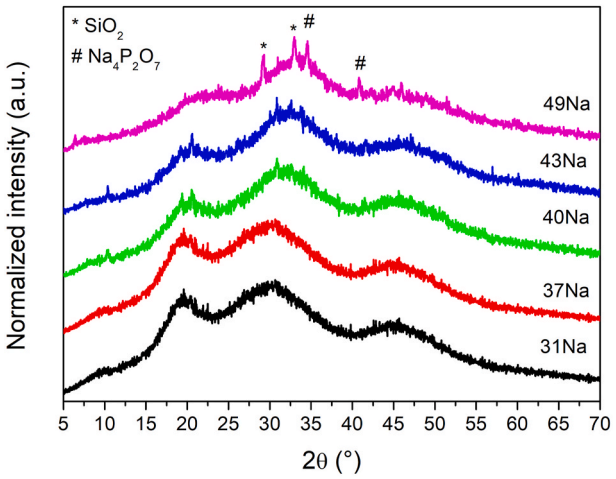


**Fig. 5.** X-ray diffractograms of the samples.

Si–*O*–B bonds [46,47]. Additionally, the band at 1094 $cm^{-1}$ is also characteristic of asymmetric stretching Si–*O*–Si bonds [46,48]. The next in intensity, also broad and asymmetric band extends from 1250 to 1600 $cm^{-1}$. The maximum is visible at 1353 $cm^{-1}$, with a slight inflection at 1428 $cm^{-1}$ and a shoulder at 1461 $cm^{-1}$. These bands, merging into one broad band, are associated with the symmetric stretching relaxation of the B–O bands of the $BO_3$ trigonal units [44,45,47]. In this wavenumber range, silicate units and a small amount of phosphate units are not active and most probably do not influence the band asymmetry. The next visible, low-intense band around 713 $cm^{-1}$ can be associated with the bending vibration of bridging oxygen (B–*O*–B) between trigonal $BO_3$ groups, which are active within the mid-region (500–800 $cm^{-1}$) [38,44]. However, the symmetric stretching vibration of O–Si–O can also be active in this region [50]. A small band visible around 574 $cm^{-1}$ is assigned to $\nu$(P–O) bonding in $(PO_4)^{3-}$ [49]. Most likely, the phosphate units form isolated forms and do not combine with the borate and silicate units. A broad band centered at 481 $cm^{-1}$ corresponds to the Si–*O*–Si bending vibration characteristic of the silicate network $[SiO_4]^{4-}$ [50,51].

Knowing that in the samples, the increase in Na content led mainly decrease in the B content, the observed changes in the IR spectra can be correlated to the progressive depolymerization of the borate network. In sample 31Na, the modifier content was 17.3 at%, and the glass network composed of 21 at% B and over 5 at% Si with 1 at% P. In such a situation, a strongly fragmented glass network is anticipated. In the subsequent sample, the sodium content increased to approximately 21 at%. As a result, the band in the IR spectrum shifted to the lower wavenumbers, notably evident for the two dominant bands as shown in Fig. 6B. As the glass network undergoes further substitution with increasing sodium contents, a continued progressive shift of the main bands is observed. Most of these changes can be primarily correlated to the decreasing boron content in the structure. Additionally, the silicon content is also reduced to a lesser extent. Consequently, for the 49Na sample with the highest sodium content and the lowest boron content, a change in the shape of the dominant band (~982 $cm^{-1}$) can be observed, from one wide band to two separated bands. Moreover, the band that was previously barely visible around 1200 $cm^{-1}$ in sample 31Na becomes an intense band with two maxima for the 49Na sample. The very wide band at the highest wavelengths has also narrowed. Notable, changes in the appearance of the band at 730 $cm^{-1}$, related to the presence of silicon, becomes sharper for the 49Na sample, suggesting the appearance of a crystalline phase. This result is in agreement with the XRDs findings. A similar trend is visible for the band associated with the presence of phosphorus also for samples 43Na and 40Na. The bands associated with the borate units remained rounded.

### 3.2. Thermal properties

Based on the obtained DSC curves (Fig. 7A), the values of the glass transition temperature ($T_g$) as indicated by the endothermic drift, and the onset temperature of the exothermic process correlated with the crystallization process were determined. The presence of only one glass transition temperature is typical for glasses in which phase separation does not occur. Analyzing the $T_g$ values of the glass, presented in Fig. 7B (depicted by black squares), a clear descending trend as evident as the sodium content increases. This observed trend suggests a strong

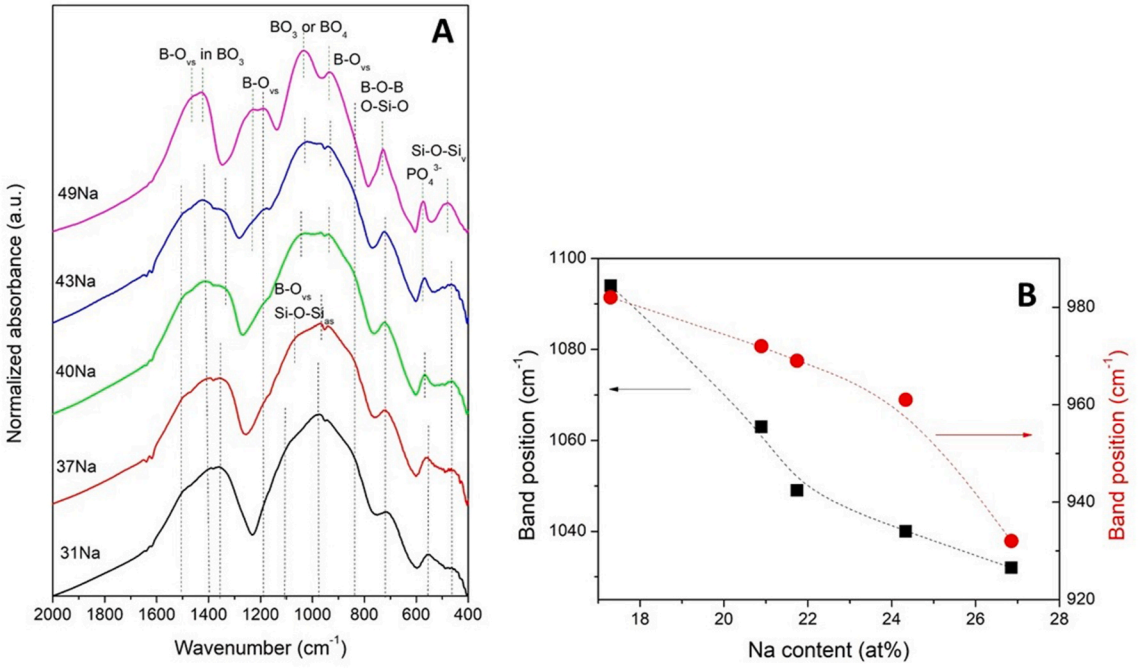


**Fig. 6.** (A) FTIR spectra of the glasses and (B) the biggest systematic shift of the two dominant bands associated with the substitution of two glass-crosslinking oxides by modifying sodium, the breaked lines are for eye guidance.

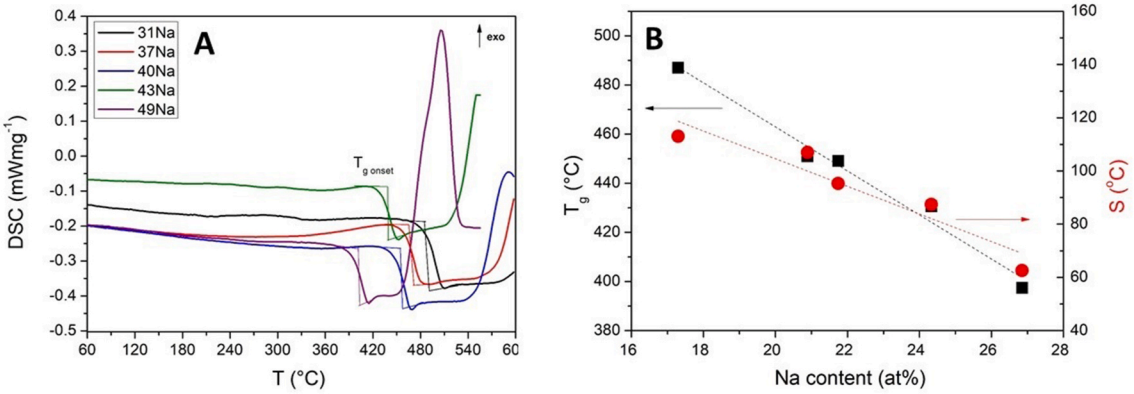


**Fig. 7.** (A) DSC curves for all glasses and (B) glass transition temperature (black squares) and thermal stability (red circles) as a function of Na content. (For interpretation of the references to color in this figure legend, the reader is referred to the Web version of this article.)

influence of sodium, leading to a weakening of the glass matrix structure due to the depolymerization of the silicate-borate glass bonds, and the formation of non-bridging oxygens [1,50,52]. This mechanism works by substituting the more energy-demanding bridging bonds with less energy-consuming bonds that do not bridge oxygen. Sodium, being an alkali element, possesses low ionization energy, facilitate the release of an electron and create ionic compounds. In silicate and borate glasses, sodium disrupts the Si–O and B–O bonds and creates non-bridging bonds, consequently decreasing both the melting temperature and the glass transition temperature [1,21]. Additionally, thermal stability (*S*) was estimated as the difference between the crystallization onset temperature and glass transition temperature. The values of thermal stability are shown in Fig. 7B (depicted by red circles). Again, a clear correlation is observed between the thermal stability of the glass and the sodium content in the glasses. This demonstrates that the increase in sodium content shifts the onset of the crystallization process from 600°C (31Na), through 558°C (37Na), 544°C (40Na), and 518°C (43Na), to the lowest temperature of 460°C (49Na). These observations and relationships highlights a significant impact of sodium content on the possibility of inhomogeneous mixing or insolubility of raw material components among themselves in melted samples. Particularly for the 49Na sample, which contains the highest amount of sodium, achieving a completely homogenous and amorphous sample was unattainable.

### 3.3. Electrical properties

The sample with composition $Na_{26.9}B_{16.4}Si_{4.4}P_{0.9}Al_1O_{50.5}$ prepared with a high Na content of 49mol% was difficult to melt into a shape suitable for electrical properties measurements, and is therefore excluded from further impedance spectroscopy tests.

The behavior of the real and imaginary parts as a function of frequency is studied across all temperatures, with each subsequent samples analyzed separately. In all samples, it was observed that the dependence of the real part of the impedance tended to zero at high frequencies. As the frequency decreased, an increase to a certain maximum value and subsequent stabilization in the lower frequency range was observed. For higher temperatures, an additional increase in the lowest frequencies can be observed. The imaginary part of the impedance shows a maximum typical for the relaxation process, correspondingly in the middle of the increase in the real part of the impedance. Moreover, an increase was visible for the lowest frequencies in the higher temperature range. The phenomenon of increasing both components in the lowest frequency range is quite often observed in ionic conductors and is correlated with the process of ion accumulation at the electrodes, known as the electrode process. The maximum observed for the imaginary part of the impedance appeared asymmetric and broad, suggesting the occurrence of more than one relaxation process [54,55]. Similar spectra were observed for higher and lower temperatures, respectively, with the relaxation process shifting towards lower and higher frequencies, respectively. In the case of samples 31Na and 37Na, the process extended beyond the range of tested frequencies at temperatures below 263K, while for samples 40Na and 43Na, it occurred at temperatures below 313K.

The observed behavior was further analyzed based on Nyquist plots, which present the relationship between the imaginary and the real part of the impedance. Fig. 8 illustrates Nyquist plots for two samples: 31Na ((A) and (B)) with the lowest sodium content and 43Na ((C) and (D)) with the highest sodium content, at temperatures of 273 K and 363 K. In each case, a semicircle is visible, however, its widened and flattened shape may suggest the presence of two overlapping semicircles. Similar spectra were observed in the remaining samples. The presence of two separate semicircles is particularly visible in the temperature range from approximately 273 K–383 K, as shown in Fig. 9 for samples (B) 37Na, (C) 40Na and (D) 43Na. As the temperature changes, the semicircles move and their proportions change. At higher temperatures, the high-frequency semicircle is no longer visible, and for lower temperatures, the low-frequency semicircle beyond the measured frequency range. The two semicircles are associated with the occurrence of two relaxation processes. Moreover, for higher temperatures and lower frequencies, an electrode process is observed, characterized by onset of third process. The presence of two relaxation processes may be related to the occurrence of two different conduction processes. It is possible that two different carriers may be transported within the material, or one type of carrier may move through two different areas within the sample. In these materials, the conduction process is caused by the jump of sodium ions in the glass network [4,7-9,11]. Structural studies have shown that samples 31Na and 37Na have a granular structure (in the nano scale), which suggests the occurrence of a phase agglomeration, likely with a higher sodium content. In such a situation, two relaxation processes may be associated to conduction through region richer and poorer in sodium ions. In samples 40Na and 43Na, nanocrystallization of the sodium-rich region take place. Consequently, in these samples, the process of conduction of sodium ions through nanocrystallites and the surrounding glass matrix occurs.

Hence, impedance analysis was conducted for all samples using an equivalent circuit of two R-CPE (R resistor and CPE constant phase element connected in parallel) circuits connected in series. The equivalent impedance of one circuit is described by the Cole-Cole relation [54, 55]:

$$Z^* = \frac{R}{1 + (j\omega\tau)^{1-\alpha}} \quad (1)$$

Where '$Z^*$' is the complex impedance, '$R$' is the resistance of a process, '$\tau$' is the mean dielectric relaxation time, '$\omega$' is the angular frequency,

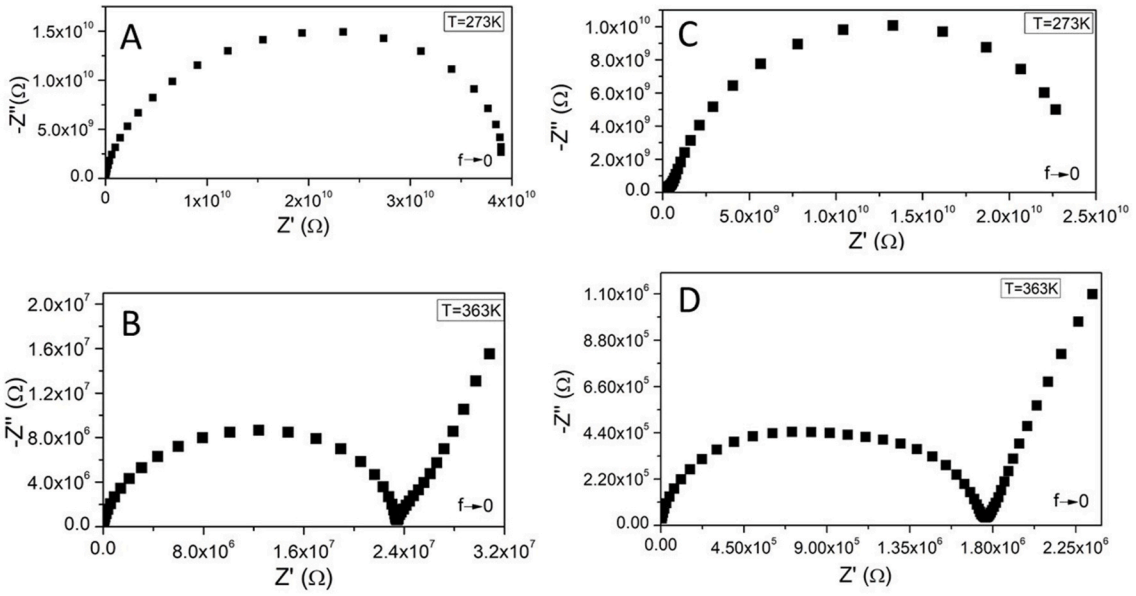


**Fig. 8.** Nyquist plots (imaginary versus real part of impedance) for representative samples with the lowest (31Na (A) and (B)) and highest (43Na (C) and (D)) sodium content, measured at two temperatures 273 K and 363 K.

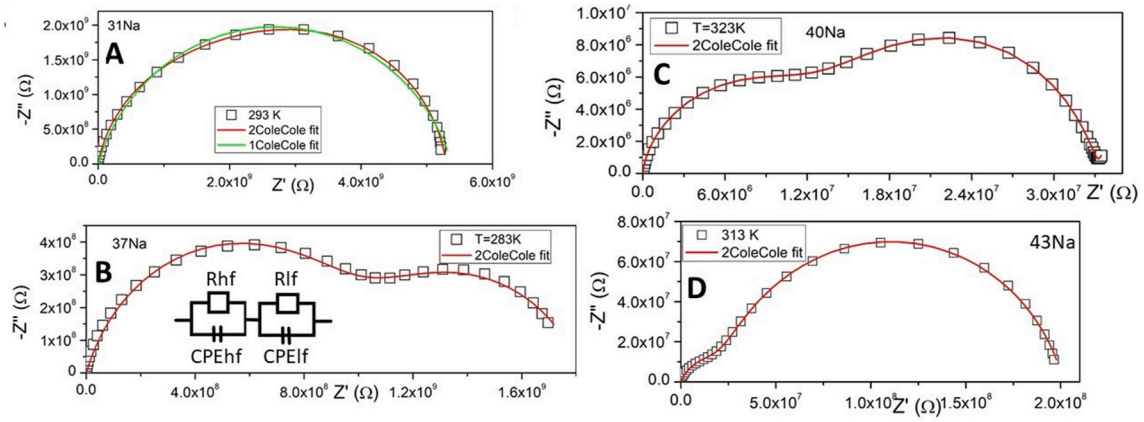


**Fig. 9.** Nyquist plots for samples (A) 31Na (293 K), (B) 40Na (283 K), (C) 37Na (323 K), and (D) 43Na (413 K) along with the result of fitting equivalent electrical circuit consisting of two R-CPE. The green-lines present the fitting of one ColeCole relation, red-lines present the fitting of two ColeCole equations connected in series, as shown in Fig B. (For interpretation of the references to color in this figure legend, the reader is referred to the Web version of this article.)

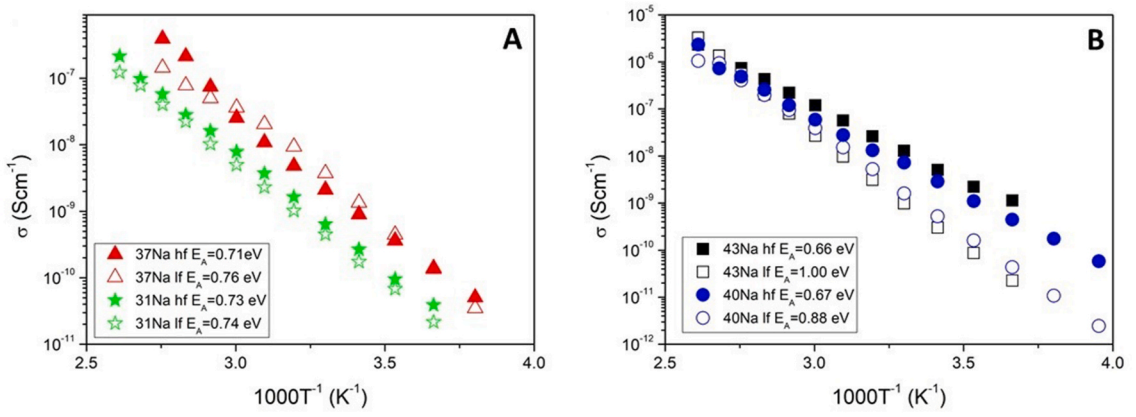


**Fig. 10.** Conductivities and activation energies of relaxation processes occurring at high ('hf') and low ('lf') frequencies, obtained from fitting Nyquist plots (Fig. 8), for A) samples 31Na and 37Na, and B) samples 40Na and 43Na.

and 'α' > 0 is a parameter describing the width of the relaxation time distribution. The equivalent circuit was selected to separate the conduction processes occurring in different areas of the sample. The fitting results are shown as red-lines in Fig. 9. For the 31Na sample, in which one semicircle is theoretically visible, the fitting was performed using one R-CPE circuit, but the fitting deviated significantly from the raw data (green lines in Fig. 9A). Only when employing two circuits did the fitting yield satisfactory results, suggesting the presence of two overlapping semicircles (red lines in Fig. 9 (A)). Based on the obtained resistances and samples dimensions, the conductivity values of two relaxation processes occurring in each sample were determined. These two processes were respectively termed 'hf' as a process occurring at high frequencies and characterized by lower relaxation times, and 'lf' as a process occurring at lower frequencies described by higher relaxation times. The obtained conductivities are illustrated in Fig. 10 (A and B), along with the estimated activation energies using Arrhenius law:

$$\sigma T = \sigma_0 \exp\left(-\frac{E_A}{kT}\right) \quad (2)$$

The '$\sigma_0$' is the conductivity pre-exponential factor, '$E_A$' denotes the activation energy for the long-range diffusion of mobile ions and '$k$' is the Boltzman's constant [56]. For 31Na sample, it can be observed that the conductivities describing both processes are similar and have the same activation energy of approximately 0.73 eV. However, they are characterized by different relaxation times with parameters 'α' close to 0.1. The 37Na sample also shows a similar situation, with slightly higher conductivities than the 31Na sample. However, the 'α' parameters range from 0.1 to 0.3, remaining lower for higher temperatures and the 'hf' process. The results for samples 31Na and 37Na indicate that two relaxation processes are related to the transport of sodium ions through two distinct regions, with one likely being richer in sodium ('hf' process). Conversely, samples 40Na and 43Na show conductivities for both processes differing by an order of magnitude in the low temperature range, while their conductivity values are similar in high temperature range. However, the activation energies for 'hf' is lower and approximately 0.67 eV and for 'lf' it increases to 1 eV for the 43Na sample. Moreover, the 'α' parameter ranges between 0.1 and 0.3 for these samples, with no visible trend. In the case of samples 40Na and 43Na, the conduction process occurs through the nanocrystallites ('hf' process) and the surrounding glassy matrix ('lf' process).

Fig. 11 presents the frequency dependence of the real part of conductivity (σ′) at different temperatures for exemplar glasses: 31Na (Fig. 11 (A)) and 43Na (Fig. 11 (B)). Each glass sample exhibits two distinct parts: DC, which is frequency independent, and AC, which is frequency dependent. In all cases, it can be seen that the range of the DC section increases with temperature. Moreover, for high temperatures T = 363K and T = 413K, at low frequency region below 1 Hz, the glasses show a decrease in conductivity which is closely associated with the electrode effect. The conductivity spectra were analyzed using the Jonscher relation to estimate the DC conductivity. Where the real part of conductivity is expressed by: $\sigma' = \sigma_{DC} + A\omega^s$, where 'A′ is constant and 's' is the temperature and frequency-dependent parameter [53]. The results of fitting the Jonscher relation to the obtained conductivity spectra are shown in Fig. 11 (as black lines). It is noteworthy that the matching of the AC part was satisfactory for samples only at certain temperatures. This is attributed to the observation of an additional relaxation process that creates the ripple [56]. Therefore, fitting the Jonscher relation was only employed to determine the value of DC conductivity of all samples.

The $\sigma_{DC}$ values (obtained from Fig. 11) are presented in Fig. 12 (A) for all glass samples. It is evident that the DC conductivity increases with temperature across all samples over the entire temperature range, consistent with Arrhenius' law (relation 2). The values of $\ln\sigma_0$ and $E_A$ determined from the fits (Fig. 12 (A) with equation (2)) and $\sigma_{DC}$ (estimated at temperatures of 273 K and 363 K) are summarized in Table 2. At low temperatures, $\sigma_{DC}$ values range from $10^{-11}$ to $10^{-12}$ $Scm^{-1}$, with no clear correlation between sodium content and conductivity. However, at the highest measured temperatures 423 K a typical dependence of the increase in DC conductivity with the sodium ion content becomes evident, as shown in Fig. 12 (B). Notably, 43Na sample show the highest conductivity at a temperature of 423 K of $10^{-5}$ $Scm^{-1}$. The observed dependencies may be related to the mobility of sodium ions, which is higher at higher temperature. For low temperatures, the thermal energy is too low to effectively cause most carriers in the samples to jump. Analysis of Table 2 data reveals, that the activation energy initially decreases as the $Na_2O$ content increases from 31 to 37 mol%, and then begins to increase for higher contents from approximately 0.7 eV to almost 1 eV. The magnitude of activation energy observed is typical for an ion hopping mechanism. Sodium ions are mobile ions in the glass matrix and typically the conductivity increases with increasing charge carrier concentration. However, if the concentration of carriers is too high, there is a problem with the movement of free carriers. The packing density of the previously loose glass network becomes too clogged and the free transfer of ions becomes difficult [4]. For this reason, an increase in activation energy can be observed.

## 4. Conclusions

Five borophosphosilicate glass samples with varying sodium contents were synthesized and characterized. Glasses with up to 37 mol% $Na_2O$ were found to be transparent with granular structure. Beyond this threshold, an agglomeration phenomenon occurred, leading to the formation of nanosize crystalline phases of $SiO_2$ and $Na_4P_2O_7$. The main structural units comprising the glass network are $BO_3$ and $BO_4$ borate

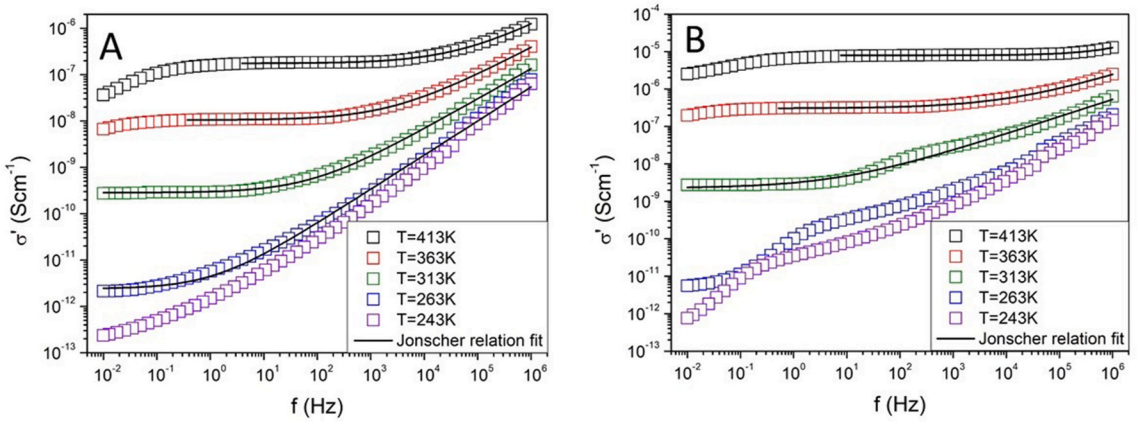


**Fig. 11.** The frequency dependence of the real part of conductivity at different temperatures for glasses: (A) 31Na and (B) 43Na.

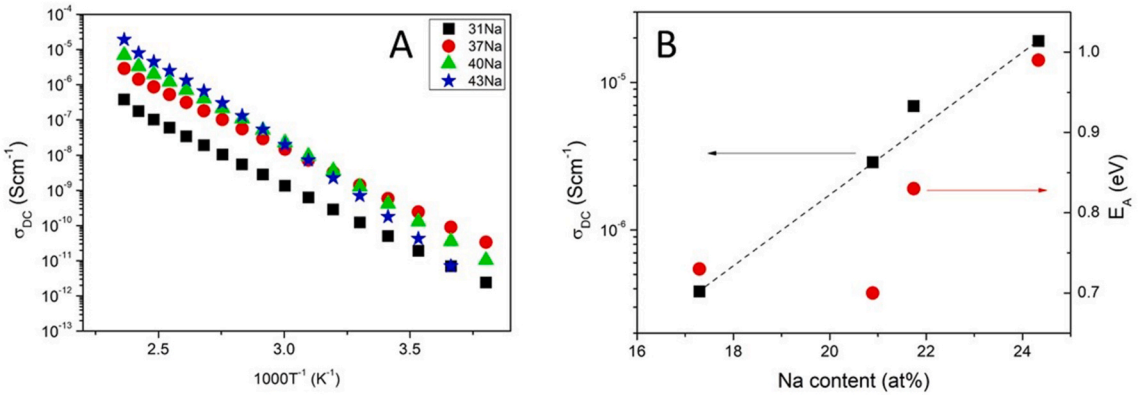


**Fig. 12.** (A) DC conductivity versus reciprocal temperature for all glasses. (B) DC conductivity values (obtained at 423 K) and $E_A$ as a function of sodium content.

**Table 2**
DC conductivity values at 273 and 363 K, activation energy and ln$\sigma_0$ parameter, estimated using relation 2 and Fig. 12(A).

| ID | DC conductivity | | | |
|---|---|---|---|---|
| | $\sigma_{DC}$ at 273 K (Scm$^{-1}$) ±2 % | $\sigma_{DC}$ at 363 K (Scm$^{-1}$) ±2 % | $E_A$ (eV) ±2 % | ln$\sigma_0$ (KScm$^{-1}$) ±5 % |
| 31Na | $6.96 \times 10^{-12}$ | $1.05 \times 10^{-8}$ | 0.73 | 11.07 |
| 37Na | $8.97 \times 10^{-11}$ | $1.03 \times 10^{-7}$ | 0.70 | 12.29 |
| 40Na | $3.57 \times 10^{-11}$ | $2.16 \times 10^{-7}$ | 0.83 | 16.87 |
| 43Na | $7.08 \times 10^{-12}$ | $3.04 \times 10^{-7}$ | 0.99 | 22.29 |

units, with the presence of silicate and phosphate units is also observed. The addition of sodium ions causes the depolymerization of the borate network as evidence by shifts in vibrations bands associated with the borate units. Thermal analysis revealed that increasing sodium ion content decreases the glass transition temperature, which is also correlated with a decrease in their thermal stability. Electrical properties analysis showed that the materials are ionic conductors, facilitating simultaneous transport of sodium ions. The DC conductivity increased with sodium content at high temperature range (above 333 K). However, activation energy displayed a predominantly increasing tendency with high sodium ion content, resulting in reduced effective hopping within the glass network.

## CRediT authorship contribution statement

**Zuzanna Milewczyk:** Data curation, Formal analysis, Investigation, Methodology, Conceptualization. **Sharafat Ali:** Visualization, Writing – review & editing. **Piotr Okoczuk:** Investigation, Methodology, Writing – review & editing. **Jacek Ryl:** Investigation, Methodology. **Ryszard J. Barczyński:** Visualization, Writing – review & editing. **Natalia A. Wójcik:** Conceptualization, Data curation, Formal analysis, Investigation, Methodology, Project administration, Software, Supervision, Visualization, Writing – original draft.

## Declaration of competing interest

The authors declare that they have no known competing financial interests or personal relationships that could have appeared to influence the work reported in this paper.

## References

[1] S. Saravanan, S. Rajesh, R. Palani, Thermal and structural properties of mixed alkali and transition metal ions in sodium borate glass, International Journal of Recent Research and Review 8 (2) (2015).
[2] M.A.M. Uosif, A.M.A. Mostafa, S.A.M. Issa, H.O. Tekin, Z.A. Alrowaili, O. Kilicoglu, Structural, mechanical and radiation shielding properties of newly developed tungsten lithium borate glasses: an experimental study, J. Non-Cryst. Solids 532 (2020) 119882.
[3] E. Kavaz, N.Y. Yorgun, Gamma ray buildup factors of lithium borate glasses doped with minerals, J. Alloys Compd. 752 (2018) 61.
[4] M. Tijaria, Y. Sharma, V. Kumar, S. Dahiya, J. Dalal, Effect of $Na_2O$ on physical, structural and electrical properties of borate glasses, Mater. Today: Proc. 45 (2021) 3722.
[5] N. Berwal, S. Dhankhar, P. Sharma, R.S. Kundu, R. Punia, N. Kishore, Physical, structural and optical characterization of silicate modified bismuth-borate-tellurite glasses, J. Mol. Struct. 1127 (2017) 636.
[6] V. Thakur, A. Singh, R. Punia, S. Dahiya, Lakhwant Singh, Structural properties and electrical transport characteristics of modified lithium borate glass ceramics, J. Alloys Compd. 696 (2017) 529.
[7] M. Dawy, A.H. Salama, Electrical and optical properties of some sodium borate glasses, Mater. Chem. Phys. 71 (2001) 137.
[8] N.A. Wójcik, M. Prześniak-Welenc, P. Kupracz, J. Karczewski, M. Gazda, R. J. Barczyński, Mixed ionic–electronic conductivity and structural properties of strontium-borate glass containing nanocrystallites of $Bi_2VO_{5.5}$, Phys. Status Solidi 254 (2017) 1700093.
[9] N.A. Szreder, P. Kupracz, M. Prześniak-Welenc, J. Karczewski, M. Gazda, K. Siuzdak, R.J. Barczyński, Electronic and ionic relaxations in strontium–borate glass and glass-ceramics containing bismuth and vanadium oxides, Solid State Ionics 282 (2015) 37.
[10] G.W. Morey, The Properties of Glasses, second ed., Reinhold, New York, 1954, p. 465.
[11] N.A. Wójcik, P. Kupracz, R.J. Barczyński, B. Jonson, S. Ali, Ion conduction in beryllium-alumino-silicate glasses doped with sodium or sodium and lithium ions, Solid State Ionics 341 (2019) 115055.
[12] Sayed Yousef El, Sayed Mostafa El, A. El-Adawy, Optical and electrical properties of borate glasses in the system: $B_2O_3/Na_2O/TiO_2$, J. Appl. Sci. 6 (2006) 1292.
[13] E. Kavaz, An experimental study on gamma ray shielding features of lithium borate glasses doped with dolomite, hematite and goethite minerals, Radiat. Phys. Chem. 160 (2019) 112.
[14] S. Gandi, V. Satya Chidambara Swamy Vaddadi, S. Srihari Sripada Panda, N. Kumar Goona, S. Reddy Parne, M. Lakavat, A. Bhaumik, Recent progress in the development of glass and glass-ceramic cathode/solid electrolyte materials for next-generation high capacity all-solid-state sodium-ion batteries: a review, J. Power Sources 521 (2022) 230930.
[15] R. Zheng, X. Zhou, Y. Yang, Q. Wu, P. Lv, K. Yu, W. Wei, Effects of heat treatment on Na-ion conductivity and conduction pathways of fluorphosphate glass-ceramics, J. Non-Cryst. Solids 471 (2017) 280.
[16] Y. Zhao, F. Tong, C. Fan, S. Yu, B. Han, J. Gao, Y. Lou, P. Jiang, Z. Wang, Quasi-solid sodium ions electrolyte of $Na_2O$-$B_2O_3$-$SiO_2$-$H_2O$ system hydrated glass, Bull. Mater. Sci. 43 (2020) 1.
[17] S. Song, H.M. Duong, A.M. Korsunsky, N. Hu, L. Lu, A $Na^+$ superionic conductor for room-temperature sodium batteries, Sci. Rep. 6 (2016) 1.
[18] N.A. Wójcik, B. Jonson, R.J. Barczyński, P. Kupracz, D. Möncke, S. Ali, Electrical properties of $Na_2O$-CaO-$P_2O_5$ glasses doped with $SiO_2$ and $Si_3N_4$, Solid State Ionics 325 (2018) 157.
[19] J.A. Dutta, T.P. Sinha, P. Jena, S. Adak, Ac conductivity and dielectric relaxation in ionically conducting soda–lime–silicate glasses, J. Non-Cryst. Solids 354 (2008) 3952.
[20] J. Du, A.N. Cormack, The medium range structure of sodium silicate glasses: a molecular dynamics simulation, J. Non-Cryst. Solids 349 (2004) 66.
[21] R. Hanna, The structure of sodium silicate glasses and their far-infrared absorption spectra, The Journal of Physical Chemistry 69 (1965) 3846.
[22] M. Lopes, J.E. Shelby, Introduction to Glass Science and Technology, second ed., Royal Society of Chemistry, Cambridge CB4 OWF, UK, 2007, p. 308.
[23] A. Dutta, T.P. Sinha, P. Jena, S. Adak, Ac conductivity and dielectric relaxation in ionically conducting soda–lime–silicate glasses, J. Non-Cryst. Solids 354 (2008) 3952.
[24] M.J. Lakin, H. Scholze, Glass: Nature, Structure, and Properties, Springer, New York, 2012.

[25] G. Fuxi, L. Fengying, G. Donghong, Physical properties of glasses containing several glass-forming oxides, J. Non-Cryst. Solids 80 (1986) 468.
[26] M.L. Braunger, C.A. Escanhoela, I. Fier, L. Walmsley, E.C. Ziemath, Electrical conductivity of silicate glasses with tetravalent cations substituting Si, J. Non-Cryst. Solids 358 (2012) 2855.
[27] S. Ali, N.A. Wójcik, B. Jonson, E.I. Kamitsos, X. Li, J. Luo, D. Möncke, Synthesis, structural characterization and thermal properties of Ca and La doped soda-lime glasses by laser melting, Int. J. Appl. Glass Sci. 11 (2020) 699.
[28] N.A. Wójcik, S. Ali, E.I. Kamitsos, D. Möncke, Niobate in silicate and phosphate glasses: effect of glass basicity on crucible dissolution, Int. J. Appl. Glass Sci. 13 (2022) 121.
[29] X. Chi, Y. Zhang, F. Hao, S. Kmiec, H. Dong, R. Xu, K. Zhao, Q. Ai, T. Terlier, L. Wang, L. Zhao, L. Guo, J. Lou, H.L. Xin, S.W. Martin, Y. Yao, An electrochemically stable homogeneous glassy electrolyte formed at room temperature for all-solid-state sodium batteries, Nat. Commun. 13 (2022) 2854.
[30] Y. Ruan, F. Guo, J. Liu, S. Song, N. Jiang, B. Cheng, Optimization of $Na_3Zr_2Si_2PO_{12}$ ceramic electrolyte and interface for high performance solid-state sodium battery, Ceram. Int. 45 (2019) 1770.
[31] T. Honma, M. Okamoto, T. Togashi, N. Ito, K. Shinozaki, T. Komatsu, Electrical conductivity of $Na_2O$–$Nb_2O_5$–$P_2O_5$ glass and fabrication of glass–ceramic composites with NASICON type $Na_3Zr_2Si_2PO_{12}$, Solid State Ionics 269 (2015) 19.
[32] A.M. Nieto-Munoz, J.F. Ortiz-Mosquera, A.C. Rodrigues, Novel sodium superionic conductor of the $Na_{1+y}Ti_2Si_yP_{3-y}O_{12}$ series for application as solid electrolyte, Electrochim. Acta 319 (2019) 922.
[33] N.A. Wójcik, S. Wolff, J. Karczewski, J. Ryl, S. Ali, Effect of crystallinity on structural, thermal, and in vitro dissolution properties of $Na_2O$-CaO-$Nb_2O_5$/MgO-$P_2O_5$ glass-ceramics, J. Eur. Ceram. Soc. 5 (2023) 2234.
[34] S. Schuller, P. Benigni, S. Gossé, S. Bégaud-Bordier, G. Mikaelian, R. Podor, J. Rogez, Liquid-liquid phase separation in borosilicate glass enriched in $MoO_3$ – experimental investigations and thermodynamic calculations, J. Non-Cryst. Solids 600 (2023) 121997.
[35] O.V. Mazurin, Phase Separation in Glass, North-Holland, 1984.
[36] Werner Vogel, Chemistry of Glass, The American Ceramic Society, 1985.
[37] P. Kupracz, J. Karczewski, M. Prześniak-Welenc, N.A. Szreder, M.J. Winiarski, T. Klimczuk, R.J. Barczyński, Microstructure and electrical properties of manganese borosilicate glasses, J. Non-Cryst. Solids 423–424 (2015) 68.
[38] D. Möncke, E.I. Kamitsos, A. Herrmann, D. Ehrt, M. Friedrich, Bonding and ion–ion interactions of $Mn^{2+}$ ions in fluoride–phosphate and boro-silicate glasses probed by EPR and fluorescence spectroscopy, Journal of Non-Crystalline Solid 357 (2011) 2542.
[39] L. Levien, C.T. Prewitt, Structure and elastic properties of quartz at pressure, Am. Mineral. 66 (1981) 324.
[40] I. Tordjman, M. Bagieu-Beucher, R. Zilber, Zeitschrift für Kristallographie, Kristallgeometrie, Kristallphysik, Kristallchemie 140 (1974) 145.
[41] F. Holder Cameron, Raymond E. Schaak, Tutorial on powder X-ray diffraction for characterizing nanoscale materials, ACS Nano 13 (2019) 7359.
[42] L. Balachander, G. Ramadevudu, Md Shareefuddin, R. Sayanna, Y.C. Venudhar, IR analysis of borate glasses containing three alkali oxides, Sci. Asia 39 (2013) 278.
[43] K.M. Al-Mokhtar, FTIR and optical absorption studies of $[B_2O_3]$-$[Na_2O]$-$[Li_2O]$-[CuO] doped with $[MgF_2]$ nanoparticle, Journal of Nanotechnology & Advanced Materials 8 (2020) 45.
[44] N. Kishore Sanjay, A. Agarwal, Investigation of structural, optical and transport properties of $MoO_3$–PbO–$B_2O_3$ glasses, J. Alloys Compd. 487 (2009) 52.
[45] A.A. El-Kheshen, F.H. El-Batal, S.Y. Marzouk, UV-visible, infrared and Raman spectroscopic and thermal studies of tungsten doped lead borate glasses and the effect of ionizing gamma irradiation, Indian J. Pure Appl. Phys. 46 (2008) 225.
[46] G. Shao, X. Wu, Y. Kong, S. Cui, X. Shen, C. Jiao, J. Jiao, Thermal shock behavior and infrared radiation property of integrative insulations consisting of $MoSi_2$/borosilicate glass coating and fibrous $ZrO_2$ ceramic substrate, Surf. Coating. Technol. 270 (2015) 154.
[47] Ch Gautam, A. Kumar Yadav, A. Kumar Singh, A review on infrared spectroscopy of borate glasses with effects of different additives, Int. Sch. Res. Notices 17 (2012) 428497.
[48] S. Ali, J. Ryl, A.S. Hakeem, K. Grochowska, N.A. Wójcik, Investigation of the structural and thermal properties of aluminum-rich Ca–Al–Si–O–N glasses, Prog. Solid State Chem. 71 (2023) 100414.
[49] J. Dziewanowska, J. Karczewski, S. Ali, N.A. Wójcik, Nanocrystallization as a tool for controlling in vitro dissolution of borophosphate glass, Ceram. Int. 49 (2023) 27382.
[50] N.A. Wójcik, S. Ali, A. Mielewczyk-Gryń, B. Jonson, Two-step synthesis of niobium doped Na–Ca–(Mg)–P–Si–O glasses, Journal of Matererial Science 56 (2021) 7613.
[51] P. Okoczuk, M. Łapiński, T. Miruszewski, P. Kupracz, L. Wicikowski, Changes on the surface of the $SiO_2$/C composite, leading to the formation of conductive carbon structures with complex nature of DC conductivity, Materials 14 (2021) 2158.
[52] N.A. Wójcik, S. Ali, D. Möncke, N.S. Tagiara, E.I. Kamitsos, H. Segawa, M. Eriksson, B. Jonson, The influence of Be addition on the structure and thermal properties of alkali-silicate glasses, J. Non-Cryst. Solids 521 (2019) 119532.
[53] A.K. Jonscher, Dielectric relaxation in solids, J. Phys. Appl. Phys. 32 (1999) R57.
[54] J.R. Macdonald, Impedance spectroscopy, Ann. Biomed. Eng. 20 (1992) 289.
[55] S.R. Elliott, A.P. Owens, The diffusion-controlled relaxation model for ionic transport in glasses, Phil. Mag. B 60 (1989) 777.
[56] A.S. Nowick, A.V. Vaysleyb, W. Liu, Identification of distinctive regimes of behaviour in the ac electrical response of glasses, Solid State Ionics 105 (1998) 121.